$Co(OH)_2$ nanosheet-decorated graphene–CNT composite for supercapacitors of high energy density

2014 Sci. Technol. Adv. Mater. 15 014206

(http://iopscience.iop.org/1468-6996/15/1/014206)

OPEN ACCESS
IOP Publishing | National Institute for Materials Science
Science and Technology of Advanced Materials
Sci. Technol. Adv. Mater. **15** (2014) 014206 (6pp)
doi:10.1088/1468-6996/15/1/014206

$Co(OH)_2$ nanosheet-decorated graphene–CNT composite for supercapacitors of high energy density

Qian Cheng[1,2], Jie Tang[1,2], Norio Shinya[1] and Lu-Chang Qin[3]

[1] National Institute for Materials Science, 1-2-1 Sengen, Tsukuba 305-0047, Japan
[2] Doctoral Program in Materials Science and Engineering, University of Tsukuba, 1-1-1 Tennodai, Tsukuba 305-8577, Japan
[3] Department of Physics and Astronomy, University of North Carolina at Chapel Hill, Chapel Hill, NC 27599-3255, USA

E-mail: tang.jie@nims.go.jp

Received 31 July 2013
Accepted for publication 21 November 2013
Published 17 January 2014

Abstract

A composite of graphene and carbon nanotubes has been synthesized and characterized for application as supercapacitor electrodes. By coating the nanostructured active material of $Co(OH)_2$ onto one electrode, the asymmetric supercapacitor has exhibited a high specific capacitance of 310 F g^{-1}, energy density of 172 Wh kg^{-1} and maximum power density of 198 kW kg^{-1} in ionic liquid electrolyte EMI-TFSI.

Keywords: supercapacitor, graphene, carbon nanotube, cobalt hydroxide

1. Introduction

The supercapacitor is a promising energy storage device since it can deliver a power density several orders of magnitude higher than a lithium-ion battery, which has been the most advanced energy storage device up to now [1, 2]. In addition, the excellent cycle life and its safety in operation make it highly competitive in many applications such as in electric and hybrid vehicles [3]. Some of the recently developed nanostructured carbon structures, such as carbon nanobeads, carbon nanotubes (CNTs), carbon nanohorns and especially graphene, have a high specific surface area, high electrical conductivity and good chemical stability [4–10]. The theoretical specific surface area of graphene is 2630 m^2 g^{-1}, which is much larger than that of the activated carbon and CNTs that are usually used in electrochemical double-layer capacitors, although the Brunauer–Emmett–Teller specific surface area of activated carbon could reach as high as 3000 m^2 g^{-1}, largely owing to the presence and contributions of functional groups in activated carbon [3]. Graphene can interface with electrolyte ions on both of its sides and has the best structure for energy storage (figure 1(a)). However, there are also issues with pristine graphene electrodes. Firstly, the chemically reduced graphene usually has an electrical conductivity of about 100–200 S m^{-1}, which is two orders of magnitude lower than that of conductive single-walled CNTs (usually 10 000 S m^{-1}) [11]. Secondly, like most nanomaterials, graphene is also prone to irreversible agglomeration or to restack into graphite through van der Waals interactions during the drying process that is used to obtain it. In this case, it would be difficult for the electrolyte ions to gain access to the inner layers to form electrochemical double layers if the graphene sheets are stacked together. Instead, the electrolyte ions could only accumulate on the top and the bottom surfaces of the graphene stack, which would then lead to a lower specific capacitance since the stacked material cannot be fully utilized, as illustrated in figure 1(d) [12]. Thirdly, a graphene electrode cannot function well without a binder, which would usually reduce the specific capacitance.

We have recently studied and developed a graphene–CNT composite with a three-dimensional porous network structure that has exhibited record-high energy density and power density when used in an electrochemical double-layer

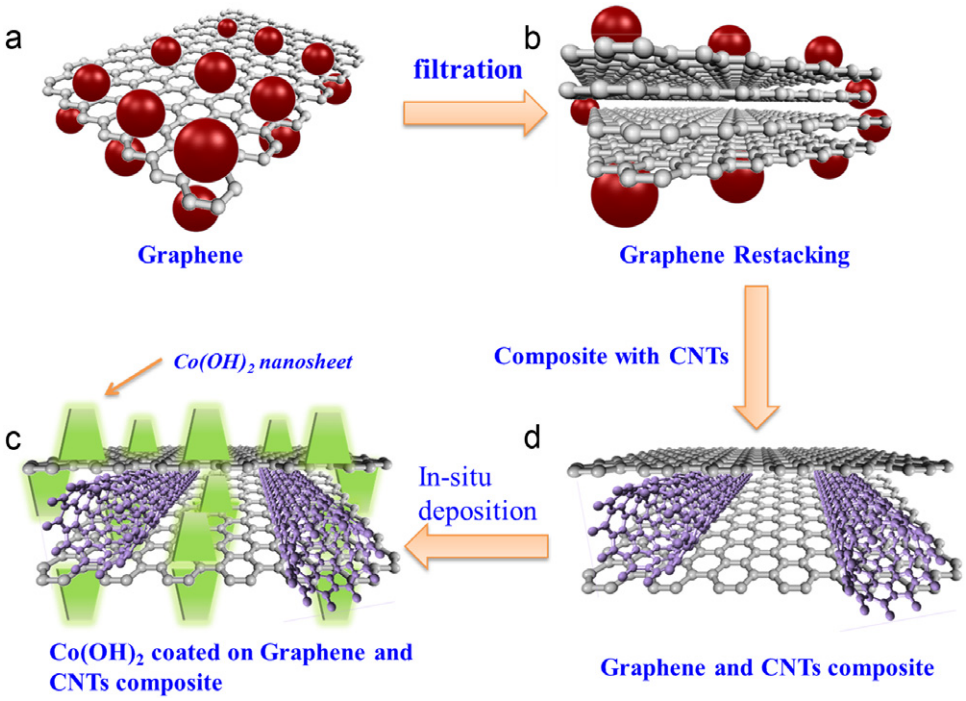

Figure 1. Schematic of graphene-based electrodes. (a) Single-layer graphene. Single-layer graphene has the highest surface area of 2630 $m^2\,g^{-1}$, which can interface with electrolyte ions on both sides of the graphene. (b) Few-layer graphene. Graphene nanosheets are likely to agglomerate through van der Waals interactions during the drying process. It would be difficult for electrolyte ions to access the ultra-small pores, especially for larger ions such as those in an organic electrolyte, or at a high charging rate. (c) Graphene–CNT composite is coated with vertically aligned $Co(OH)_2$ nano-sheets by cathodic *in situ* deposition to fabricate a graphene–CNT–$Co(OH)_2$ composite. (d) Graphene–CNT composite. CNTs can serve as a spacer between the graphene nanosheets to provide rapid diffusion pathways for the electrolyte ions; moreover, they can increase the electrical conduction. The CNTs also serve as a binder to hold the graphene nanosheets together, preventing the disintegration of the composite in electrolyte.

capacitor [13]. However, the specific capacitance as well as the energy density will be further increased if we can decorate the graphene–CNT composite structure with nanostructured active materials such as transition metal oxides, hydroxides or conductive polymers. Among the active materials, metal oxides and hydroxides have been considered the most promising for electrochemical supercapacitors since they often show an extremely high specific capacitance [14–21]. Cobalt hydroxide ($Co(OH)_2$) is an excellent example material due to its layered structure with large internal spaces for fast insertion and desertion of electrolyte ions [22]. Its high theoretical specific capacitance of 3458 $F\,g^{-1}$ has also made it a very attractive active material for pseudocapacitors [8, 11, 23–27]. However, metal hydroxides often suffer from high electrical resistance because of the chemical nature of the material. In addition, the thick coating of active material also contributes to a poor cyclability.

We therefore designed a $Co(OH)_2$ nano-sheet–decorated graphene–CNT composite structure which is shown schematically in figure 1. First, we use suspensions of graphene and single-walled CNTs to produce a graphene–CNT composite by sonication and vacuum filtration. The graphene–CNT composite is designed to have high conductivity, chemical stability and a three-dimensional structure with high porosity, as illustrated in figure 1(d). The porous structure of the graphene–CNT composite is to facilitate the diffusion of the electrolyte into electrodes to provide channels for rapid ion transport. The vertically aligned $Co(OH)_2$ nano-sheets are then coated onto the graphene–CNT composite by electrodeposition. The $Co(OH)_2$-coated graphene–CNT composite electrodes are utilized binder-free. The vertically aligned $Co(OH)_2$ nano-sheets can further shorten the ion diffusion path. The nano-structured active material can also increase the efficiency of usage of materials since only the part within a few nanometers from the surface of the active material can take part in the redox reactions and contribute to the actual device capacitance.

2. Experimental details

2.1. Graphene oxide

Graphene oxide was synthesized using a modified Hummers–Offeman method from graphite in our experiment [28]. Graphite and $NaNO_3$ were first mixed together in a flask before H_2SO_4 was added to the flask, which was kept and stirred in an ice bath. Potassium permanganate was then added to the suspension. The color of the suspension would become bright brown. After H_2O_2 was added to dilute the suspension, the mixture was finally washed by rinsing with 5% HCl and demonized water. After centrifugation, filtration and drying in a vacuum, graphene oxide was obtained in the form of a black powder.

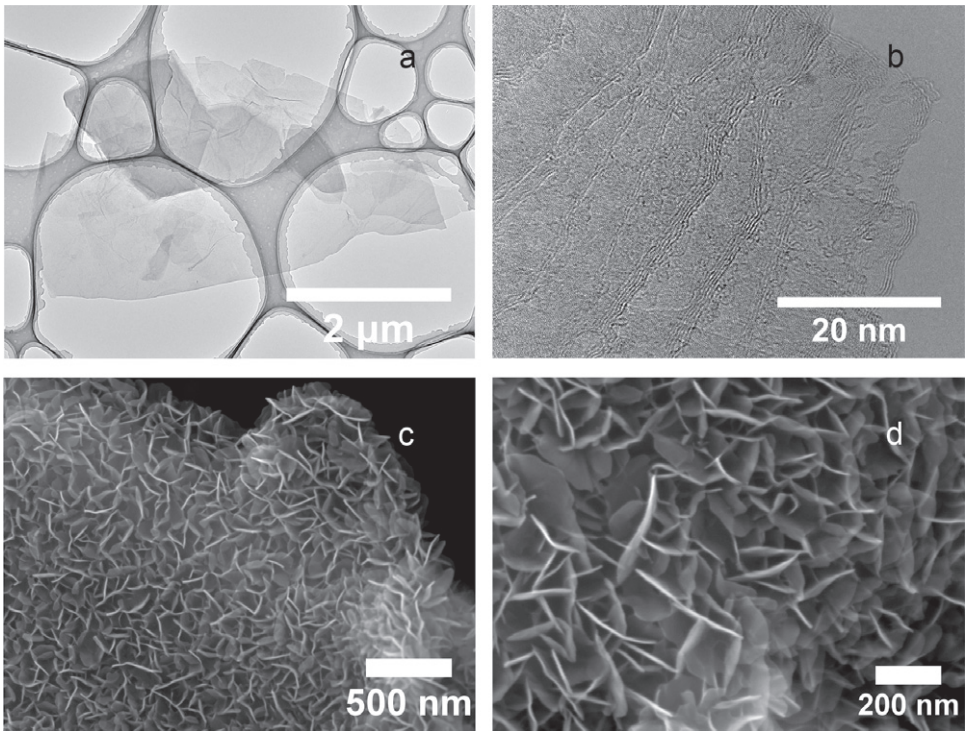

Figure 2. Morphological characterization of graphene-based structures. (a) TEM image of as-synthesized graphene at low magnification showing several overlapping graphene flakes. (b) TEM image of as-synthesized graphene at high magnification revealing the number of graphene layers in the few-layer graphene structure. (c) SEM image of a graphene–CNT composite with vertically aligned $Co(OH)_2$ nanosheets' coating at low magnification. (d) SEM image of $Co(OH)_2$ coating at high magnification. The thickness of the $Co(OH)_2$ nanosheet is approximately 10 nm.

2.2. Reduction of graphene oxide

The graphene oxide suspension was heated to 100 °C and hydrazine hydrate was added to the suspension. The suspension was then reduced and black powders were collected by filtration. The obtained material was then washed using distilled water again to remove the excessive hydrazine and was redistributed into water for sonication and centrifugation. The final graphene material was collected by vacuum filtration.

2.3. Graphene–CNT–Co(OH)$_2$ composite

To make the graphene–CNT–$Co(OH)_2$ composite, graphene and CNTs were first dispersed and mixed in ethanol to obtain a uniform graphene–CNT composite film by vacuum filtration. The electrodeposition of $Co(OH)_2$ nano-sheets was conducted using a three-electrode system, and a platinum sheet ($1 \times 2\,cm^2$) was used as the counter electrode. Cathodic deposition was controlled by an potentiostat in 0.1 M $CoCl_2$ electrolyte containing 10% ethanol [29]. The $Co(OH)_2$ nano-sheets were synthesized in two steps: (i) the nucleation of $Co(OH)_2$, performed at a constant current at room temperature; and (ii) the growth of the $Co(OH)_2$ nano-structures under a constant current.

2.4. Electrochemical and structural characterization

The electrochemical properties and capacitance of the super-capacitor electrodes were evaluated in a two-electrode setup by cyclic voltammetry (CV), galvanostatic charge and discharge, and electrochemical impedance spectroscopy (EIS). The CV response of the electrodes was measured at different scan rates varying from 10 to 100 mV s^{-1}. The graphene–CNT and graphene–CNT–$Co(OH)_2$ composites were studied in the ionic liquid of 1-ethyl-3-methylimidazoliumbis(trifluoromethanesulfone)imide (EMI-TFSI) with a potential window wider than 4.5 V in comparison with Li/Li^+ [30]. EIS measurements were carried out with a dc bias sinusoidal signal of 0.005 V over the frequency range of 100 kHz–0.1 Hz. The morphologies and nanostructure were examined using scanning electron microscopy (SEM, JSM-6500) and transmission electron microscopy (TEM, JEM-2100).

3. Results and discussion

Figure 2 shows the morphologies of graphene and the graphene–CNT–$Co(OH)_2$ composite. Figure 2(a) displays a TEM image of the as-synthesized graphene, in which thin sheets of graphene are clearly resolved. A high-resolution TEM image of graphene is shown in figure 2(b), revealing that this few-layer graphene is flat, a feature considered essential for achieving a high value of specific surface area. The CNTs used in this composite structure have higher electrical conductivity than the chemically reduced graphene, and in effect the electrical resistance of the electrode is reduced, i.e. the CNTs act as the 'pathways' for electrical conduction. In addition, the CNTs can also serve as spacers in-between the graphene nano-sheets to enhance electrolyte ion accessibility.

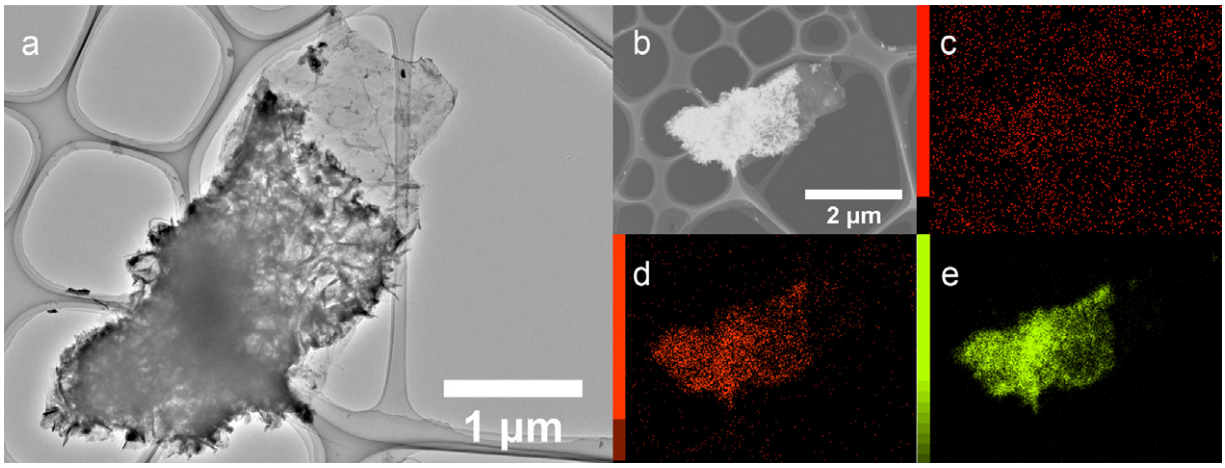

Figure 3. TEM image and elemental mapping of $Co(OH)_2$-coated graphene. (a) TEM image of $Co(OH)_2$-coated few-layer graphene. (b) Dark-field image of the same $Co(OH)_2$-coated graphene piece combined with maps of carbon (c), oxygen (d) and cobalt (e).

Figure 2(c) is an SEM image after $Co(OH)_2$ coating. The vertically aligned $Co(OH)_2$ nano-sheets were grown on graphene quite uniformly. We controlled the thickness of the $Co(OH)_2$ coating by simply adjusting the coating time. This structure is expected to improve the power performance since the vertically aligned $Co(OH)_2$ nano-sheets are grown directly on the surface of graphene to ensure good contact with the graphene. A high-resolution SEM image of the $Co(OH)_2$ nano-sheets is given in figure 2(d), showing a uniform coating of $Co(OH)_2$. The thickness of the $Co(OH)_2$ nano-sheets is around 10 nm.

Figure 3(a) shows graphene with a $Co(OH)_2$ coating. We can observe that the $Co(OH)_2$ nano-sheets are still on the surface of the graphene after sonication was applied in the preparation of the TEM sample, indicating that we can make a robust composite by *in situ* deposition. An elemental mapping was carried out on the same piece of sample. Although the carbon mapping was not helpful because of the amorphous carbon film on the copper grid (figure 3(c)), the $Co(OH)_2$ coating is well revealed by the elemental mapping of oxygen and cobalt, which is shown in figures 3(d) and (e), respectively.

The capacitance of an electrode is sensitive to the cell configuration used for the electrochemical measurement, and it is always significantly higher when using a three-electrode system [31]. A two-electrode test cell was therefore used in this work because it can provide the most accurate measurement of the material performance of the supercapacitor [32]. We used an ionic liquid electrolyte EMI-TFSI for a higher operating (charging/discharging) voltage. Figure 4(a) shows the CV curves of graphene–CNT supercapacitor in EMI-TFSI at different scan rates ranging from 10 to 200 mV s^{-1}. The symmetric and hysteretic CV loops indicate excellent charge propagation in the electrodes. As we know, the shape of the CV loop of an ideal capacitor should be rectangular if the contact resistance is small. A larger resistance distorts the loop and results in a narrower loop with an oblique angle. Figure 4(b) shows the galvanostatic charge/discharge curves of the composite electrode at charging currents of 1 and 2 mA. Both charging curves show a relatively flattened plateau after 3.7 V. This is due to the reactions with the functional groups present on the electrode when it was charged to such a high voltage. We obtained a specific capacitance of 310 F g^{-1} at 1 mA (1 A g^{-1}) and 100 F g^{-1} at 2 mA (2 A g^{-1}) with a maximum energy density of 172 Wh kg^{-1}. Figure 4(c) is the Nyquist plot of impedance collected in the frequency range between 100 kHz and 0.01 Hz for the graphene–CNT–$Co(OH)_2$ composite. As expected from a supercapacitor at low frequency, the imaginary part increases sharply and a nearly vertical line is observed, indicating a predominantly capacitive behavior in action. As the frequency increases, the influence of the electrode porosities is observed as indicated by a constant phase element typified by the Warburg curve [33]. The EIS curve shown in figure 4(c) is nearly linear in the low-frequency region, and has a semi-circular shape in the high-frequency region, from which the interfacial leakage resistance, R_F, due to overcharge or faradaic redox reactions caused by impurities or functional groups, can be deduced with a simplistic model. The smaller the R_F, the greater the kinetic reversibility of the faradaic reactions. In a practical supercapacitor, to a good approximation, it can be regarded as being composed of a non-faradaic current for electrochemical double-layer charging in parallel with some faradaic current component through R_F. We can learn that the graphene–CNT–$Co(OH)_2$ composite has a small charge-transfer resistance. The equivalent series resistance (ESR) of 8.2 Ω for the supercapacitor with the graphene–CNT and the graphene–CNT–$Co(OH)_2$ electrodes was obtained from the Z1-intercept. The maximum power density p_{max} was calculated by $p_{max} = V_{max}^2/(4mR_{ESR})$, where R_{ESR} is the equivalent series resistance, m is the total weight of the two electrodes and V_{max} is the maximum charging voltage. Using $V_{max} = 4$ V for the EMI-TFSI electrolyte, the obtained maximum power density for the graphene–CNT and graphene–CNT–$Co(OH)_2$ supercapacitor was 198 kW kg^{-1}. Figure 4(d) shows the cycling performance of the asymmetric supercapacitor with a $Co(OH)_2$ coating of 1 mg cm^{-2} at a charging current density of 2 A g^{-1}. The capacitance dropped by 30% after 1500 cycles, showing reasonable performance

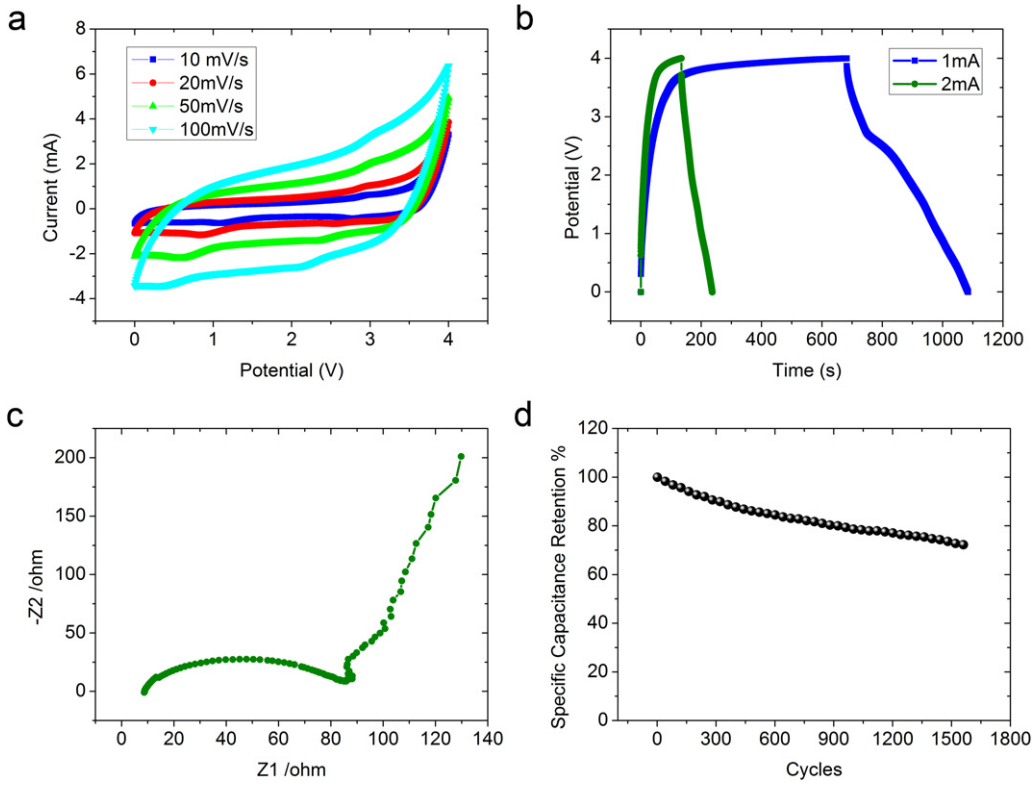

Figure 4. Electrochemical properties of $Co(OH)_2$ coated graphene–CNT composite. (a) CV curves of graphene–CNT–$Co(OH)_2$ composite at different scan rates ranging from 10 to 100 mV s^{-1} in EMI-TFSI electrolyte. (b) Galvanostatic charge/discharge curves of the composite at charging currents of 1 and 2 mA. (c) Nyquist plot of EIS data of graphene–CNT–$Co(OH)_2$ composite electrode. (d) Cycling performance of graphene–CNT–$Co(OH)_2$ composite at charging density of 2 A g^{-1}.

for an asymmetric supercapacitor, where pseudocapacitance must also have contributed to the device performance due to the coated $Co(OH)_2$ from the redox reaction $Co(OH)_2 + TFSI^- \rightarrow CoOOH + HTFSI + e^-$.

4. Conclusions

We have fabricated graphene–CNT and graphene–CNT–$Co(OH)_2$ electrodes and assembled them in asymmetric supercapacitors. The single-walled CNTs act as a conductive spacer as well as a conductive binder in this composite structure. A high energy density of 172 Wh kg^{-1} and a maximum power density of 198 kW kg^{-1} were obtained.

Acknowledgments

This work was supported by JSPS Grants-in-Aid for Scientific Research numbers 19310081 and 22310074, JST ALCA Program and the Nanotechnology Network Project of the Ministry of Education, Culture, Sports, Science and Technology (MEXT), Japan.

References

[1] Simon P and Gogotsi Y 2008 Materials for electrochemical capacitors *Nature Mater.* **7** 845–54
[2] Miller J R and Simon P 2008 Materials science—electrochemical capacitors for energy management *Science* **321** 651–2
[3] Zhang L L and Zhao X S 2009 Carbon-based materials as supercapacitor electrodes *Chem. Soc. Rev.* **38** 2520–31
[4] Frackowiak E and Beguin F 2001 Carbon materials for the electrochemical storage of energy in capacitors *Carbon* **39** 937–50
[5] Frackowiak E and Beguin F 2002 Electrochemical storage of energy in carbon nanotubes and nanostructured carbons *Carbon* **40** 1775–87
[6] Futaba D N, Hata K, Yamada T, Hiraoka T, Hayamizu Y, Kakudate Y, Tanaike O, Hatori H, Yumura M and Iijima S 2006 Shape-engineerable and highly densely packed single-walled carbon nanotubes and their application as super-capacitor electrodes *Nature Mater.* **5** 987–94
[7] Wang Y, Shi Z Q, Huang Y, Ma Y F, Wang C Y, Chen M M and Chen Y S 2009 Supercapacitor devices based on graphene materials *J. Phys. Chem.* C **113** 13103–07
[8] Stoller M D, Park S J, Zhu Y W, An J H and Ruoff R S 2008 Graphene-based ultracapacitors *Nano Lett.* **8** 3498–502
[9] Wang D W, Li F, Zhao J P, Ren W C, Chen Z G, Tan J, Wu Z S, Gentle I, Lu G Q and Cheng H M 2009 Fabrication of graphene/polyaniline composite paper via *in situ* anodic electropolymerization for high-performance flexible electrode *ACS Nano* **3** 1745–52
[10] Pandolfo A G and Hollenkamp A F 2006 Carbon properties and their role in supercapacitors *J. Power Sources* **157** 11–27
[11] Park S and Ruoff R S 2009 Chemical methods for the production of graphenes *Nature Nanotechnol.* **4** 217–24
[12] Yan J, Wei T, Shao B, Fan Z, Qian W, Zhang M and Wei F 2010 Preparation of a graphene nanosheet/polyaniline composite with high specific capacitance *Carbon* **48** 487–93

[13] Cheng Q, Tang J, Ma J, Zhang H, Shinya N and Qin L-C 2011 Graphene and carbon nanotube composite electrodes for supercapacitors with ultra-high energy density *Phys. Chem. Chem. Phys.* **13** 17615–24
[14] Fischer A E, Pettigrew K A, Rolison D R, Stroud R M and Long J W 2007 Incorporation of homogeneous, nanoscale MnO_2 within ultraporous carbon structures via self-limiting electroless deposition: implications for electrochemical capacitors *Nano Lett.* **7** 281–6
[15] Chang J K, Lee M T, Tsai W T, Deng M J, Cheng H F and Sun I W 2009 Pseudocapacitive mechanism of manganese oxide in 1-ethyl-3-methytimidazolium thiocyanate ionic liquid electrolyte studied using x-ray photoelectron spectroscopy *Langmuir* **25** 11955–60
[16] Babakhani B and Ivey D G 2010 Anodic deposition of manganese oxide electrodes with rod-like structures for application as electrochemical capacitors *J. Power Sources* **195** 2110–7
[17] Cheng Q, Tang J, Ma J, Zhang H, Shinya N and Qin L-C 2011 Graphene and nanostructured MnO_2 composite electrodes for supercapacitors *Carbon* **49** 2917–25
[18] Conway B E 1991 Transition from supercapacitor to battery behavior in electrochemical energy-storage *J. Electrochem. Soc.* **138** 1539–48
[19] Long J W, Swider K E, Merzbacher C L and Rolison D R 1999 Voltammetric characterization of ruthenium oxide-based aerogels and other RuO_2 solids: the nature of capacitance in nanostructured materials *Langmuir* **15** 780–5
[20] Yan J, Fan Z J, Wei T, Qian W Z, Zhang M L and Wei F 2010 Fast and reversible surface redox reaction of graphene–MnO_2 composites as supercapacitor electrodes *Carbon* **48** 3825–33
[21] Li G R, Feng Z P, Ou Y N, Wu D, Fu R and Tong Y X 2010 Mesoporous MnO_2/carbon aerogel composites as promising electrode materials for high-performance supercapacitors *Langmuir* **26** 2209–13
[22] Jayashree R S and Kamath P V 1999 Electrochemical synthesis of alpha-cobalt hydroxide *J. Mater. Chem.* **9** 961–963
[23] Liang Y Y, Cao L, Kong L P and Li H L 2004 Synthesis of $Co(OH)_2$/USY composite and its application for electrochemical supercapacitors *J. Power Sources* **136** 197–200
[24] Tung V C, Allen M J, Yang Y and Kaner R B 2009 High-throughput solution processing of large-scale graphene *Nature Nanotechnol.* **4** 25–9
[25] Stankovich S, Dikin D A, Dommett G H B, Kohlhaas K M, Zimney E J, Stach E A, Piner R D, Nguyen S T and Ruoff R S 2006 Graphene-based composite materials *Nature* **442** 282–6
[26] Geim A K and Kim P 2008 Carbon wonderland *Sci. Am.* **298** 90–7
[27] Becerril H A, Mao J, Liu Z, Stoltenberg R M, Bao Z and Chen Y 2008 Evaluation of solution-processed reduced graphene oxide films as transparent conductors *ACS Nano* **2** 463–70
[28] Hummers W S and Offeman R E 1958 Preparation of graphitic oxide *J. Am. Chem. Soc.* **80** 1339
[29] Cheng Q, Tang J, Ma J, Zhang H, Shinya N and Qin L-C 2011 Polyaniline-coated electro-etched carbon fiber cloth electrodes for supercapacitors *J. Phys. Chem.* C **115** 23584–90
[30] An Y, Zuo P, Cheng X, Liao L and Yin G 2011 Preparation and properties of ionic-liquid mixed solutions as a safety electrolyte for lithium ion batteries *Int. J. Electrochem. Sci.* **6** 2398–410
[31] Frackowiak E, Khomenko V, Jurewicz K, Lota K and Beguin F 2006 Supercapacitors based on conducting polymers/nanotubes composites *J. Power Sources* **153** 413–8
[32] Khomenko V, Frackowiak E and Beguin F 2005 Determination of the specific capacitance of conducting polymer/nanotubes composite electrodes using different cell configurations *Electrochim. Acta* **50** 2499–506
[33] Portet C, Taberna P L, Simon P and Laberty-Robert C 2004 Modification of Al current collector surface by sol–gel deposit for carbon–carbon supercapacitor applications *Electrochim. Acta* **49** 905–12